

# RSC Advances



This is an *Accepted Manuscript*, which has been through the Royal Society of Chemistry peer review process and has been accepted for publication.

*Accepted Manuscripts* are published online shortly after acceptance, before technical editing, formatting and proof reading. Using this free service, authors can make their results available to the community, in citable form, before we publish the edited article. This *Accepted Manuscript* will be replaced by the edited, formatted and paginated article as soon as this is available.

You can find more information about *Accepted Manuscripts* in the [Information for Authors](#).

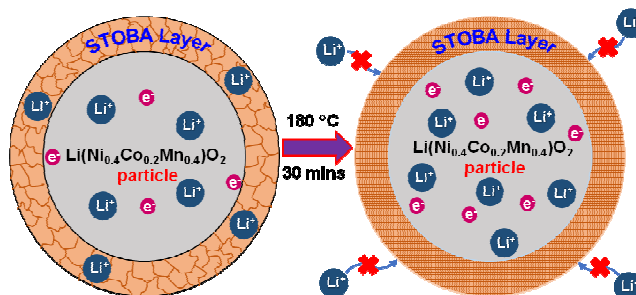
Please note that technical editing may introduce minor changes to the text and/or graphics, which may alter content. The journal's standard [Terms & Conditions](#) and the [Ethical guidelines](#) still apply. In no event shall the Royal Society of Chemistry be held responsible for any errors or omissions in this *Accepted Manuscript* or any consequences arising from the use of any information it contains.

## Graphical Abstract

Towards understanding the role of hyper-branched oligomers coated on cathode in the safety mechanism of lithium ion batteries

Hsueh-Ming Liu, Diganta Saikia, Hung-Chun Wu, Ching-Yi Su, Tsung-Hsiung Wang, Yu-Han Li, Jing-Pin Pan\* and Hsien-Ming Kao\*

The self-terminated oligomers with hyper branched architecture (STOBA) coated on the  $\text{Li}(\text{Ni}_{0.4}\text{Co}_{0.2}\text{Mn}_{0.4})\text{O}_2$  cathode material suppress thermal runaway and prevent the lithium ion batteries from explosion.



Cite this: DOI: 10.1039/c0xx00000x

www.rsc.org/xxxxxx

## ARTICLE TYPE

**Towards understanding the role of hyper-branched oligomers coated on cathode in the safety mechanism of lithium ion batteries****Hsueh-Ming Liu,<sup>a</sup> Diganta Saikia,<sup>a</sup> Hung-Chun Wu,<sup>b</sup> Ching-Yi Su,<sup>b</sup> Tsung-Hsiung Wang,<sup>b</sup> Yu-Han Li,<sup>b</sup> Jing-Pin Pan<sup>\*b</sup> and Hsien-Ming Kao<sup>\*a</sup>**

5 Received (in XXX, XXX) Xth XXXXXXXXX 20XX, Accepted Xth XXXXXXXXX 20XX  
DOI: 10.1039/b000000x

The physical and structural changes of the polymer layer, self-terminated oligomers with a hyper branched architecture (STOBA) coated on the  $\text{Li}(\text{Ni}_{0.4}\text{Co}_{0.2}\text{Mn}_{0.4})\text{O}_2$  cathode at the state of charge conditions and at different temperatures are investigated by nitrogen adsorption-desorption, X-ray photoelectron spectroscopy (XPS), resistance measurements, scanning electron microscopy (SEM) and solid-state  $^7\text{Li}$  and  $^{13}\text{C}$  NMR spectroscopy in order to improve the understanding of the role of the STOBA layer in the enhancement of the safety mechanism of lithium ion batteries. The morphological change of the STOBA layer from the porous to nonporous state around the temperature of thermal runaway of a battery is demonstrated. The change in the resistance values at high temperatures reveals that the STOBA coating is helpful for the prevention of internal short-circuit and thermal runaway. Most importantly, the  $^7\text{Li}$  NMR results acquired at a very high spinning speed (50 kHz) allow that the subtle changes in the local environments of the  $\text{Li}^+$  ions and their interaction and mobility in the STOBA-cathode interface as functions of temperature and charge states can be monitored. The combined characterization results in the present study improve the understanding of the role of the STOBA layer in the safety features of lithium ion batteries.

**Introduction**

The environmental and economical concerns toward the use of fossil fuels increase the demand for clean and renewable energy systems, such as solar cells, fuel cells, batteries and wind power generators.<sup>1-4</sup> Being powered by fossil fuels, automobiles are the one of the major sources of green house gas emitter. Therefore, transition to an electrified transportation system should be a societal goal to curb on emission. In this regards, rechargeable battery systems may provide a feasible route to achieve the objective. Various battery systems have been developed and commercialized over the past few decades.<sup>5-7</sup> Among them, the most successful rechargeable battery technology is lithium-ion battery (LIB), which has been widely used in most of today's electronic equipments and devices, and currently in electric or hybrid electric vehicles (EVs/HEVs).<sup>8-10</sup> However, the increasing use of these batteries challenges with increasing safety concerns as several cases of fire related accidents of LIBs (or packs of them) have been reported in personal electronic devices and electric vehicles. Therefore, the safety issues of LIBs are of the paramount importance.

The safety issues related to LIBs may occur under different abuse conditions, like mechanical abuse behaviors (nail penetration, drop, crush, vibration, etc.), electrochemical abuse behaviors (short circuits, overcharge, over-discharge, gas generation, etc.) and thermal abuse (external heating, flame

attack, hot combustion gases, etc.).<sup>11-12</sup> The mechanical exploitation may cause immediate failure of the battery leading to thermal runaway. The electrochemical abuse conditions such as overcharge/overdischarge or short circuits will result in the formation of dendritic lithium on the anode, dissolution of current collector, decomposition of electrolytes with gas and heat generation, and finally a thermal runaway of the battery. Moreover, the batteries experienced with external heating may undergo thermal runaway more rapidly.

To cope with the safety problems of LIBs, many protection techniques and methods have been used externally or internally. Generally, the external protection mechanism employed current interruptive devices (CID), positive temperature coefficient (PTC) devices, current limiting fuses, diodes (blocking/bypass) to minimize the potential hazards from batteries in normal operating conditions.<sup>13-15</sup> CID breaks the internal electrical connection when the internal pressure reaches a set value. PTC disks are normally put in the cell header to limit high currents. PTC elements display a large increase in resistance upon a rapid temperature rise and block the flow of current at the battery terminal. Current limiting fuses can be used when a continuous discharge is not favored. However, it is still not possible to make the Li-ion battery 100% safe because of the occasional failures of the external hardware systems mostly in abnormal conditions. Moreover, the external devices make the system complex, and add weight, volume and extra cost to the battery pack, which are not favorable for batteries with high energy or power densities.

Moreover, the external devices cannot respond quickly to the complex internal chemistry changes, such as the increase in resistance, interfacial phenomenon, corrosion of current-collectors, etc. Hence, development of a reliable internal protection mechanism is highly desirable to improve the safety of LIBs. Presently, the internal mechanism mainly focuses on improving the individual components, including cathode and anode materials, separators, current collectors, and electrolytes so as to make the battery system hazard proof.<sup>16-20</sup> The redox shuttle is one of the efficient internal protection methods that can be used to prevent the overcharge abuse in a battery.<sup>21-23</sup> In some cases, shutdown separators,<sup>24-26</sup> flame-retardant electrolyte additives,<sup>27,28</sup> thermally stable electrode materials,<sup>29,30</sup> and thermoresponsive microspheres onto anodes or separators<sup>31</sup> are used as internal protection mechanism to improve battery safety.

Among the different abuse conditions, thermal runaway has received much attention due to its harmful effect to lithium ion battery applications.<sup>32,33</sup> Thermal overheating, internal short-circuits and over-charging, leading to thermal runaway, are common safety concerns, especially among heavy-duty and high-power applications. The thermal runaway process is initiated by breakdown of solid electrolyte interphase (SEI) layer, which leads to large electrolyte reduction at the surface of the lithiated graphite anode. The cathode materials release oxygen and trigger the interfacial oxidation of the electrolytes above 180 °C, leading to a high-rate thermal runaway with a steep temperature rise, which could reach several hundred degrees within a few seconds.

To deal with the thermal runaway problem, the Industrial Technology Research Institute (ITRI) in Taiwan has successfully developed a self-terminated hyper-branched oligomer (STOBA) that can be coated on the cathode materials to suppress the risk of thermal runaway.<sup>34-36</sup> As a new material, however, the properties of STOBA are not fully studied. Lin et al. has shown that the STOBA coating dramatically reduced the thermal runaway without much affecting the electrochemical performance of LIBs.<sup>35</sup> The nail penetration test clearly showed that the STOBA coating helped to suppress the temperature from rising sharply. The temperature of the cell assembled with the bare Li(Ni<sub>0.4</sub>Co<sub>0.2</sub>Mn<sub>0.4</sub>)O<sub>2</sub> cathode without the STOBA coating was raised over 700 °C within 2 seconds.<sup>35</sup> Moreover, a rapid heat generation in a cell may be caused by accidental internal or external short-circuits. However, a detail analysis has not been carried out to understand how the STOBA layer prevents short circuits, and thus the thermal runaway in a battery. In this study, an attempt has been made to analyze the STOBA-cathode interface at the fully charged state and the structural changes of the STOBA layer at different temperatures to improve the understanding towards its safety mechanism.

## Experimental section

### Synthesis of STOBA coated cathode and anode materials

The synthesis of STOBA coated Li(Ni<sub>0.4</sub>Co<sub>0.2</sub>Mn<sub>0.4</sub>)O<sub>2</sub> materials were carried out according to the proprietary processes developed by ITRI<sup>34</sup> and also described by Lin et al.<sup>35</sup> Briefly, STOBA was dispersed in N-methyl-2-pyrrolidone (NMP, Aldrich), keeping the STOBA weight fraction of 2.0% in the mixture. Then the Li(Ni<sub>0.4</sub>Co<sub>0.2</sub>Mn<sub>0.4</sub>)O<sub>2</sub> particles (Shenzhen Tianjiao Technology

Co., Ltd) were added to the STOBA solution and stirred at 70 °C for 60 min. Afterward, a NMP solution containing polyvinylidene fluoride (PVdF, T1300, Kureha America Inc.) was added to the STOBA/Li(Ni<sub>0.4</sub>Co<sub>0.2</sub>Mn<sub>0.4</sub>)O<sub>2</sub> solution and further stirred for 30 min. Finally, the conductive agents including KS6 graphite (Timcal) and carbon black (Super P, Timcal) were added to the mixture and stirred for another 30 min. The final composition of the cathode material was 89 wt.% Li(Ni<sub>0.4</sub>Co<sub>0.2</sub>Mn<sub>0.4</sub>)O<sub>2</sub> (along with 2 wt.% STOBA in the case of the STOBA-coated sample), 4 wt.% PVdF and 7 wt.% KS6 and Super P. The resulting slurry was blade coated on aluminum foil and dried overnight in an oven to get the cathode active material. To avoid any aggregation of STOBA during the coating process, the temperature of the solution was maintained at 70 °C and a minimum amount of STOBA was used. Although the process gives very good coating layer of STOBA over the Li(Ni<sub>0.4</sub>Co<sub>0.2</sub>Mn<sub>0.4</sub>)O<sub>2</sub> particle, the layer thickness slightly varies in different regions of the particle. The anode material mesocarbon microbead (MCMB) was purchased from China Steel Chemical Corp., Taiwan. The anode active layer consisted of 95 wt.% MCMB, 1 wt.% Super P carbon and 4 wt.% PVdF binder on a Cu current collector. 1 M LiPF<sub>6</sub> in ethylene carbonate (EC)/ethyl methyl carbonate (EMC) (Zhangjiagang Guotai Huarong) (1:2 vol%) with 2 wt.% vinylene carbonate (VC) was used as the electrolyte.

### Assembling and disassembling of battery

Pouch type lithium ion battery was fabricated by using the STOBA coated Li(Ni<sub>0.4</sub>Co<sub>0.2</sub>Mn<sub>0.4</sub>)O<sub>2</sub> cathode, MCMB anode and 1 M LiPF<sub>6</sub> in EC/EMC with 2 wt.% VC as the electrolyte. A porous polyethylene film was used as separator. The battery was then charged to 100% state of charge (SOC) at 4.2 V under a constant current of 0.1C. The design capacity of pouch cell was 8 mAh. Then, the battery was disassembled in a glove box under an Ar atmosphere. The recovered STOBA coated Li(Ni<sub>0.4</sub>Co<sub>0.2</sub>Mn<sub>0.4</sub>)O<sub>2</sub> electrode with electrolyte was sealed in a high pressure Ti tube and thermally treated separately at 150 °C and 180 °C for 30 min and stored in the glove box for further characterizations.

### Characterizations

N<sub>2</sub> adsorption-desorption isotherms were measured at 77 K on a Micromeritics ASAP 2020 analyzer. The samples were degassed for 24 h before measurements. The pore size was determined from the analysis of adsorption branch of the isotherm by the Barrett-Joyner-Halenda (BJH) method. Pore volumes were obtained from the volumes of N<sub>2</sub> adsorbed at P/P<sub>0</sub> = 0.95 or in the vicinity.

Thermogravimetric analysis (TGA) was carried out under a nitrogen environment at a heating rate of 10 °C min<sup>-1</sup> from room temperature to 850 °C on a Perkin Elmer TGA7 thermogravimetric analyzer.

X-ray photoelectron spectroscopy (XPS) analysis was conducted on PHI 5000 VersaProbe (ULVAC-PHI), which employed a focused X-ray source of 30 W.

Scanning electron micrographs (SEM) of the STOBA sample at different temperatures were obtained from a FEI Nova NanoSEM 230 field-emission electron microscope at an accelerating voltage of 10 kV. Secondary electron image of the cross-sectional micrograph of the STOBA coated

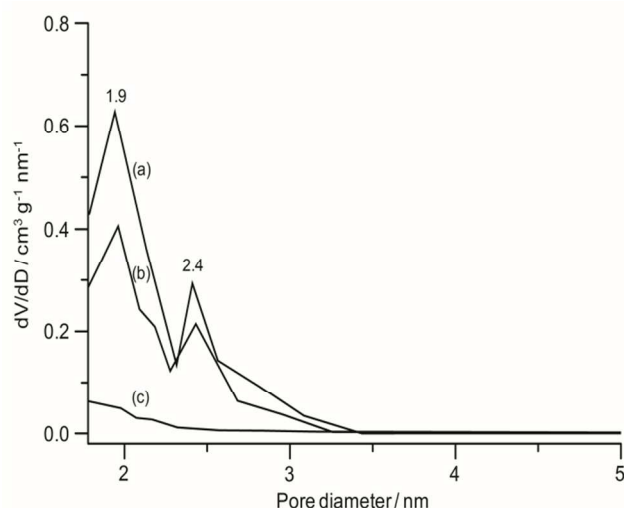


**Fig. 1** Pore size distribution curves of (a) pure STOBA, and STOBA thermally treated at (b) 150 °C and (c) 180 °C obtained from nitrogen adsorption-desorption measurements.

Li(Ni<sub>0.4</sub>Co<sub>0.2</sub>Mn<sub>0.4</sub>)O<sub>2</sub> sample was taken by focused ion beam scanning electron microscope (FIB-SEM; NOVA200 NANOLAB).

The resistance measurements of the bare and STOBA coated Li(Ni<sub>0.4</sub>Co<sub>0.2</sub>Mn<sub>0.4</sub>)O<sub>2</sub> samples were carried out in a four probe setup by using a programmable low-ohm meter DU-5010 (Delta United Instrument Co. Ltd). The recovered sample after disassembling the cell was washed with dimethyl carbonate (DMC) and dried in a vacuum chamber overnight by using a dry pump inside a glove box. The resistance of the dried sample was measured in a dry room with dew point of -40°C.

Solid-state <sup>7</sup>Li and <sup>13</sup>C NMR experiments were performed on a Varian Infinityplus-500 NMR spectrometer, equipped with Chemagnetics 1.2 mm (for <sup>7</sup>Li) and 5 mm (for <sup>13</sup>C) magic angle spinning (MAS) T3 probes. The Larmor frequencies for <sup>7</sup>Li and <sup>13</sup>C nuclei are 193.7 and 125.4 MHz, respectively. The <sup>7</sup>Li MAS spectra were acquired with a high spinning speed of 50 kHz in order to achieve better spectral resolution. The <sup>7</sup>Li chemical shift was externally referenced to 1M LiCl solution at 0 ppm. The Hartmann-Hahn matching condition for <sup>1</sup>H → <sup>13</sup>C cross-polarization (CP) MAS experiments was determined using adamantane. The <sup>13</sup>C chemical shift was externally referenced to tetramethylsilane (TMS) at 0 ppm.

## Results and discussion

### Pore size distribution and stability of STOBA

The nitrogen adsorption-desorption measurements were carried out to investigate the changes in the pore structure of the STOBA materials under thermal treatment at different temperatures. The pore size distribution of the STOBA samples at different temperatures is shown in Fig. 1. As seen in Fig. 1, the STOBA material without thermal treatment possesses a bimodal pore structure with pore sizes of 1.9 and 2.4 nm. The STOBA sample after thermal treatment at 150 °C also shows a similar bimodal pore structure. Interestingly, when the sample was thermally treated at 180 °C, no significant pores in the sample were observed. The thermal runaway of a lithium-ion battery takes

place above 180 °C due to the exothermic reaction of cathode materials and release of O<sub>2</sub>, which triggers interfacial oxidation of the electrolytes leading to a high rate of the temperature rise.<sup>11,37</sup> It was found that the porosity of STOBA almost disappeared around 180 °C as revealed by the nitrogen adsorption-desorption measurements. It suggested that the STOBA chains were crosslinked to each other and melted at high temperatures. As a result, STOBA became nonporous in nature after thermal treatment at 180 °C. The nonporous state of STOBA may restrict the direct contact of the electrolyte with oxygen and prevent the cathode-electrolyte reaction, and thus is helpful for the suppression of thermal runaway.

Thermogravimetric analysis (TGA) was carried out to measure the thermal stability of the STOBA material. The TGA curve of STOBA is shown in Fig. S1 (Electronic Supplementary Information, ESI). Initially, about 3% weight loss was observed up to 300 °C due to the small amount of physisorbed water in the STOBA sample while transferring it to the instrument. After 350 °C, the STOBA sample gradually lost weight due to the decomposition of the polymeric unit. At 850 °C, the STOBA sample retained about 48 wt.% even though the decomposition of some polymeric units. The TGA result reveals the thermal stability of the STOBA material is at least up to 300 °C, which is beneficial for preventing any heat related activity in batteries.

### XPS analysis of STOBA coated cathode

The XPS study was carried out in the fresh samples that did not undergo any charge-discharge testing. Fig. 2 displays the XPS spectra of the bare and STOBA coated Li(Ni<sub>0.4</sub>Co<sub>0.2</sub>Mn<sub>0.4</sub>)O<sub>2</sub> cathode samples. The spectrum of the STOBA coated Li(Ni<sub>0.4</sub>Co<sub>0.2</sub>Mn<sub>0.4</sub>)O<sub>2</sub> sample shows a strong N 1s peak at the binding energy of 400.2 eV due to the nitrogen attached with the fundamental building-block of STOBA.<sup>35</sup> The O 1s spectra are composed of two components at 529.6 and 531.6 eV. The main peak at 529.6 eV in the bare Li(Ni<sub>0.4</sub>Co<sub>0.2</sub>Mn<sub>0.4</sub>)O<sub>2</sub> sample is due to the characteristic O<sup>2-</sup> ions of the crystalline lattice. The second peak at 531.6 eV is attributed to the oxygen-containing species of the surface layers that have coordination deficiencies, i.e., the defects in the surface associated with sites where the coordination number of oxygen ions is smaller than in the regular sites.<sup>38</sup> The peak intensity at 531.6 eV increased and that at 529.6 eV decreased when STOBA was coated on the Li(Ni<sub>0.4</sub>Co<sub>0.2</sub>Mn<sub>0.4</sub>)O<sub>2</sub> cathode. This may be due to the increase in the surface activity as the O 1s peaks of STOBA are also expected in this binding energy range. The Co 2p spectrum shows a well defined profile with the 2p<sub>3/2</sub> and 2p<sub>1/2</sub> components at binding energies of 780.4 and 795.4 eV, respectively. The main binding energy components and small satellite peak indicates that cobalt ions are in the 3+ oxidation state in oxygen environment.<sup>37,39</sup> The Ni spectrum is characterized by an intense and complicated satellite structure. The Ni spectrum exhibits two peaks due to 2p<sub>3/2</sub> and 2p<sub>1/2</sub> at 854.4 and 872.6 eV, respectively. The low binding energy peak is in agreement with the formation of NiO, which confirms the presence of Ni<sup>2+</sup> in the compound.<sup>39</sup> The satellite peaks are about 6 eV higher energies than the main 2p<sub>3/2-1/2</sub> doublet. The wide peak centered at 854.4 eV may be due to the superposition of Ni<sup>2+</sup> and Ni<sup>3+</sup> signals. The Mn 2p spectrum depicts two distinct peaks related to Mn 2p<sub>1/2</sub> and Mn 2p<sub>3/2</sub> at binding energies of 653.6 and 642.4 eV, respectively, for the bare Li(Ni<sub>0.4</sub>Co<sub>0.2</sub>Mn<sub>0.4</sub>)O<sub>2</sub> sample.

Cite this: DOI: 10.1039/c0xx00000x

www.rsc.org/xxxxxx

## ARTICLE TYPE

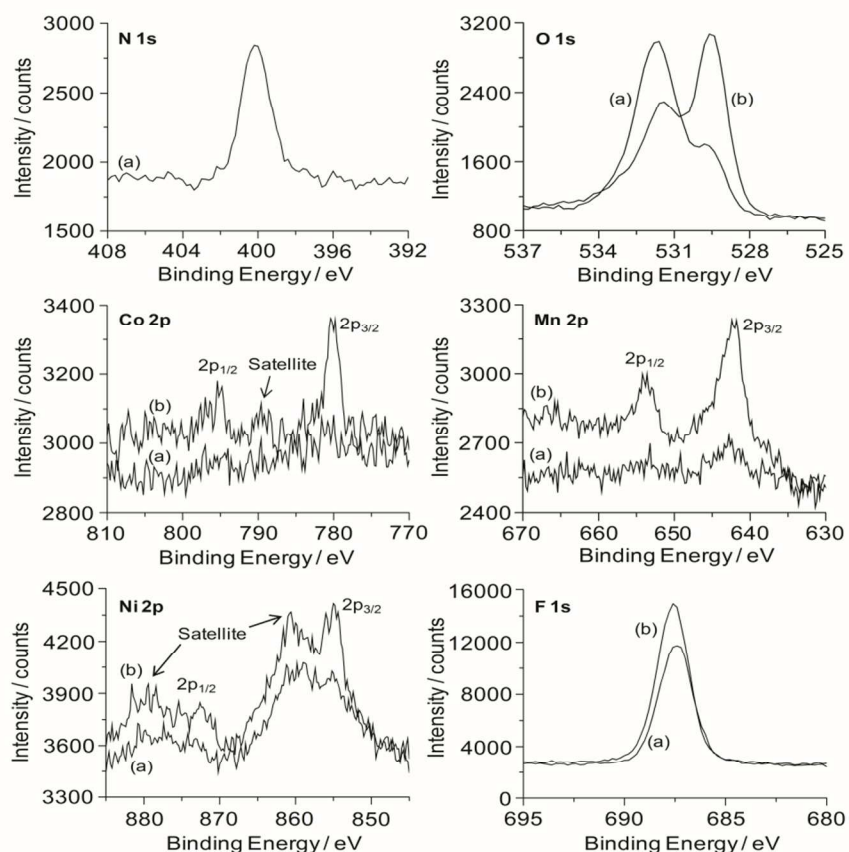


Fig. 2 XPS spectra of (a) STOBA coated  $\text{Li}(\text{Ni}_{0.4}\text{Co}_{0.2}\text{Mn}_{0.4})\text{O}_2$  cathode and (b) bare  $\text{Li}(\text{Ni}_{0.4}\text{Co}_{0.2}\text{Mn}_{0.4})\text{O}_2$  cathode with core peaks.

The two peaks of Mn  $2p_{3/2-1/2}$  doublet are assigned to the  $\text{Mn}^{4+}$  ions. The intensities of Co, Ni and Mn peaks are comprehensively reduced when STOBA was coated on the  $\text{Li}(\text{Ni}_{0.4}\text{Co}_{0.2}\text{Mn}_{0.4})\text{O}_2$  cathode, suggesting the deposition of STOBA layer on the surface of the  $\text{Li}(\text{Ni}_{0.4}\text{Co}_{0.2}\text{Mn}_{0.4})\text{O}_2$  particle (Fig. 2(a)). A strong F peak at 687.6 eV was observed because of the presence of PVdF in the cathode material as binder.<sup>38</sup> The intensity of F peak is also reduced after STOBA was coated on the surface of the  $\text{Li}(\text{Ni}_{0.4}\text{Co}_{0.2}\text{Mn}_{0.4})\text{O}_2$  particle.

To get a rough idea about the uniformity of the STOBA layer, the XPS study is also carried out to measure the intensity in three different points of the STOBA coated cathode sample with each point almost 1 cm apart from the other. The XPS spectra of the core peaks of the STOBA coated  $\text{Li}(\text{Ni}_{0.4}\text{Co}_{0.2}\text{Mn}_{0.4})\text{O}_2$  cathode sample at three different points are shown in Fig. S2 (ESI). As shown in Fig. S2, the peak intensities of the core elements at three different points are almost the same, which suggest that the STOBA layer is coated in a relatively uniform manner on the surface of the  $\text{Li}(\text{Ni}_{0.4}\text{Co}_{0.2}\text{Mn}_{0.4})\text{O}_2$  particle since XPS can explore the surface layer up to a few nanometer of depth of the sample.

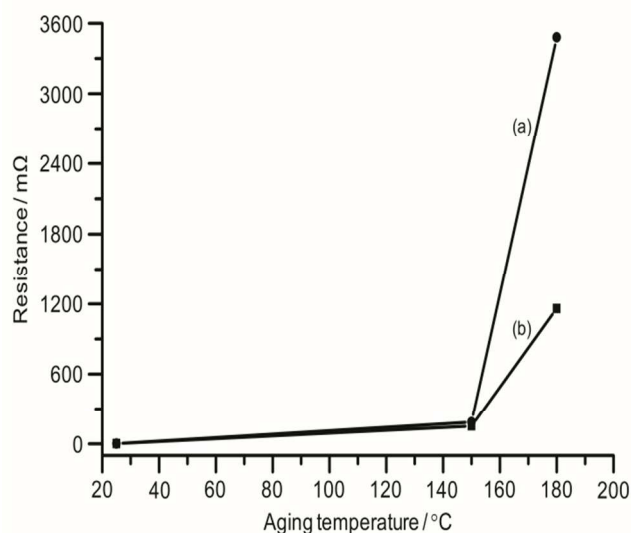
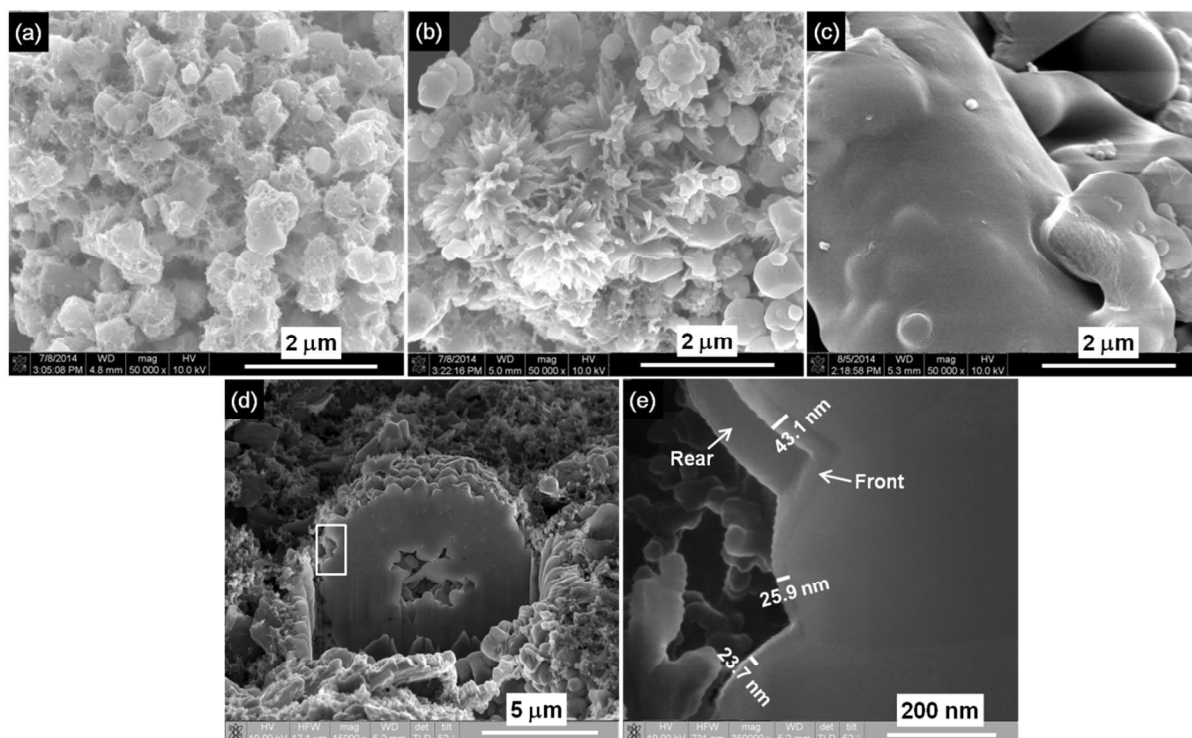


Fig. 3 Resistance measurements at different temperatures for (a) STOBA coated  $\text{Li}(\text{Ni}_{0.4}\text{Co}_{0.2}\text{Mn}_{0.4})\text{O}_2$  cathode and (b) bare  $\text{Li}(\text{Ni}_{0.4}\text{Co}_{0.2}\text{Mn}_{0.4})\text{O}_2$  cathode.

Cite this: DOI: 10.1039/c0xx00000x

www.rsc.org/xxxxxx

## ARTICLE TYPE



**Fig. 4** SEM images of STOBA material (a) without thermal treatment and with thermal treatment at (b) 150 °C and (c) 180 °C, and (d) cross-section of STOBA coated  $\text{Li}(\text{Ni}_{0.4}\text{Co}_{0.2}\text{Mn}_{0.4})\text{O}_2$  particle. The marked region of (d) is shown as an enlarged image in (e) with the STOBA coating thickness on the  $\text{Li}(\text{Ni}_{0.4}\text{Co}_{0.2}\text{Mn}_{0.4})\text{O}_2$  particle.

### 5 Resistance measurements

To understand how electrochemical behavior of the STOBA layer changes after thermal treatment at high temperatures, the resistances of the bare and STOBA coated  $\text{Li}(\text{Ni}_{0.4}\text{Co}_{0.2}\text{Mn}_{0.4})\text{O}_2$  cathodes were measured from room temperature to 180 °C. As seen in Fig. 3, both samples exhibited almost the same resistances at room temperature. The very low resistance value (~0.5 mΩ) suggests good conduction of the samples. The resistances of both samples are slowly increased with increase in temperature with a small difference in resistance values for bare  $\text{Li}(\text{Ni}_{0.4}\text{Co}_{0.2}\text{Mn}_{0.4})\text{O}_2$  cathode (152 mΩ) and STOBA coated  $\text{Li}(\text{Ni}_{0.4}\text{Co}_{0.2}\text{Mn}_{0.4})\text{O}_2$  cathode (185 mΩ) at 150 °C. After 150 °C, however, the resistance of the STOBA coated  $\text{Li}(\text{Ni}_{0.4}\text{Co}_{0.2}\text{Mn}_{0.4})\text{O}_2$  cathode sample raised sharply to 3.5 Ω in comparison to 1.2 Ω for the bare  $\text{Li}(\text{Ni}_{0.4}\text{Co}_{0.2}\text{Mn}_{0.4})\text{O}_2$  cathode at 180 °C. These resistances of the STOBA coated and bare  $\text{Li}(\text{Ni}_{0.4}\text{Co}_{0.2}\text{Mn}_{0.4})\text{O}_2$  cathode samples are 7000 and 2400 times higher than the resistances at room temperature, respectively. As the thermal runaway of a battery generally occurs around the temperature range of 150–180 °C, therefore only two temperatures of 150 °C and 180 °C were chosen, in addition to room temperature, to evaluate the resistances. Moreover, the difference in the resistance values was not very high between room temperature and 150 °C to make any significant impact on the current flow. It suggests that the bare  $\text{Li}(\text{Ni}_{0.4}\text{Co}_{0.2}\text{Mn}_{0.4})\text{O}_2$

cathode material generates oxygen and triggers interfacial oxidation around 180 °C, leading to an increase in the resistance. In the STOBA coated  $\text{Li}(\text{Ni}_{0.4}\text{Co}_{0.2}\text{Mn}_{0.4})\text{O}_2$  cathode sample, on the other hand, the STOBA material melts around that temperature and forms a dense nonporous film on the cathode surface to break the conductive network, leading to a steep rise in resistance almost 3 times higher than that of the bare  $\text{Li}(\text{Ni}_{0.4}\text{Co}_{0.2}\text{Mn}_{0.4})\text{O}_2$  cathode. This causes a drop in the current which limits the heat generation in the cell and prevents thermal runaway. Moreover, the STOBA coating prevents an internal short-circuit of the battery, which is also a crucial safety issue. As the resistance of the bare  $\text{Li}(\text{Ni}_{0.4}\text{Co}_{0.2}\text{Mn}_{0.4})\text{O}_2$  cathode is not very high at 180 °C, the cell with the bare  $\text{Li}(\text{Ni}_{0.4}\text{Co}_{0.2}\text{Mn}_{0.4})\text{O}_2$  cathode may be more prone to cause a short-circuit.

### Morphological study

The morphologies of the STOBA samples at different temperatures and the STOBA coated  $\text{Li}(\text{Ni}_{0.4}\text{Co}_{0.2}\text{Mn}_{0.4})\text{O}_2$  sample are shown in Fig. 4. As seen in Fig. 4, the STOBA material without thermal treatment exhibited the particle morphology of fibrous porous structures (Fig. 4a). After thermally treated at 150 °C, the fibrous STOBA particles started to melt, as clearly observed in Fig. 4b. When the STOBA sample was thermally treated at 180 °C, the particles were completely melted (Fig. 4c). Therefore, it can be inferred that the STOBA material

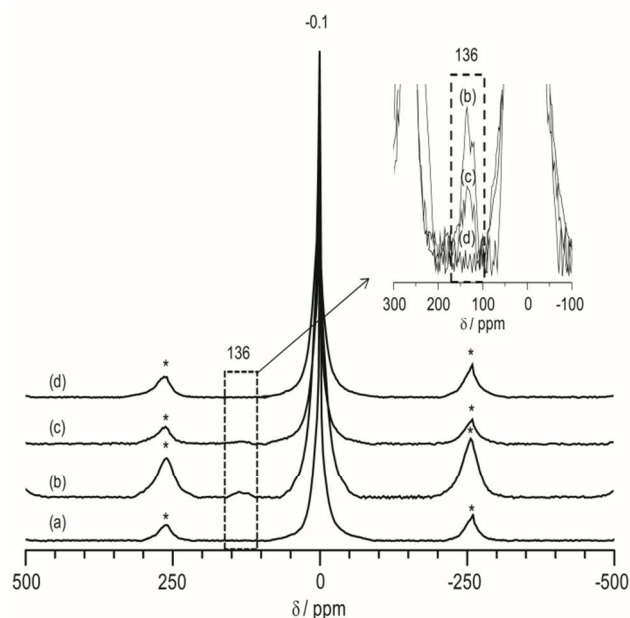


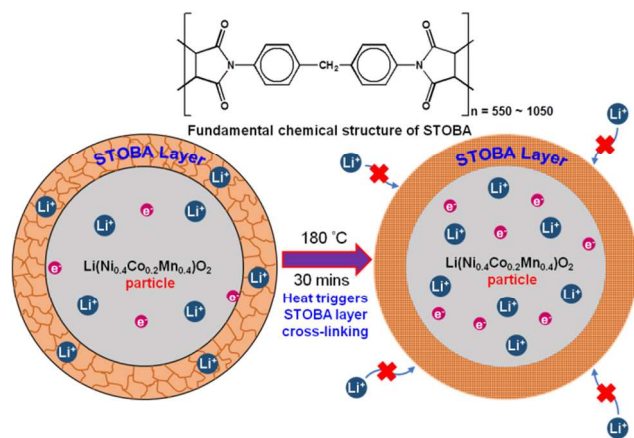
**Fig. 5**  $^7\text{Li}$  MAS NMR spectra at 100% SOC condition of (a) bare  $\text{Li}(\text{Ni}_{0.4}\text{Co}_{0.2}\text{Mn}_{0.4})\text{O}_2$  cathode, (b) STOBA coated  $\text{Li}(\text{Ni}_{0.4}\text{Co}_{0.2}\text{Mn}_{0.4})\text{O}_2$  cathode, and thermally treated (c) STOBA coated  $\text{Li}(\text{Ni}_{0.4}\text{Co}_{0.2}\text{Mn}_{0.4})\text{O}_2$  cathode at 150 °C/30 min and (d) STOBA coated  $\text{Li}(\text{Ni}_{0.4}\text{Co}_{0.2}\text{Mn}_{0.4})\text{O}_2$  cathode at 180 °C/30 min. The spinning sidebands are marked with asterisks. The inset shows the enlarged version of the 136 ppm peak.

without thermal treatment is porous enough to transport Li-ions freely, and hence does not affect the capacity significantly.<sup>35</sup> When the STOBA sample was thermally treated at 150 °C, however, the fibrous particle structure started to melt. As a result, the changes in the pore volume of the STOBA layer was slowly reduced, which is consistent with the observations revealed by the nitrogen adsorption-desorption measurements. In the case of the STOBA sample after thermal treatment at 180 °C, the fibrous STOBA particles have melted completely and the porous structure disappeared, suggesting the complete blockage of movement of lithium ions and electrons while used as a coating layer on the cathode in Li-ion batteries. Fig. 4d depicts FIB-SEM image of the cross-section of STOBA coated  $\text{Li}(\text{Ni}_{0.4}\text{Co}_{0.2}\text{Mn}_{0.4})\text{O}_2$  particle and the enlarged version of its edge is shown in Fig. 4e. The STOBA layer on the surface of  $\text{Li}(\text{Ni}_{0.4}\text{Co}_{0.2}\text{Mn}_{0.4})\text{O}_2$  particle is clearly visible with an average layer thickness of 30 nm. Based on the STOBA layer thickness and  $\text{Li}(\text{Ni}_{0.4}\text{Co}_{0.2}\text{Mn}_{0.4})\text{O}_2$  particle size, we have estimated the minimum amount of STOBA sample required to coat the  $\text{Li}(\text{Ni}_{0.4}\text{Co}_{0.2}\text{Mn}_{0.4})\text{O}_2$  particles. The detailed estimation is given in the ESI. It is found that around 0.8 wt.% of STOBA sample is sufficient to coat the  $\text{Li}(\text{Ni}_{0.4}\text{Co}_{0.2}\text{Mn}_{0.4})\text{O}_2$  particle properly. The histogram of the particle numbers vs. the particle size is given in Fig. S3 (ESI) with an inset SEM image of the bare  $\text{Li}(\text{Ni}_{0.4}\text{Co}_{0.2}\text{Mn}_{0.4})\text{O}_2$  particles. It is observed that the maximum numbers of particles are in the range of 5 to 10 nm size with a nearly spherical shape. As the estimation of the minimum amount of STOBA is carried out considering an ideal spherical cathode particle, there may be some possible errors due to the different size and shape (near spherical) of the particles as well as the different thickness of the STOBA coating layer (Fig. 4e). However, the amount of STOBA used (2 wt.%) in the present

study is more than twice the calculated amount (0.8 wt.%), which should be sufficient to coat the  $\text{Li}(\text{Ni}_{0.4}\text{Co}_{0.2}\text{Mn}_{0.4})\text{O}_2$  particle efficiently after compensating the possible errors. This established that the  $\text{Li}(\text{Ni}_{0.4}\text{Co}_{0.2}\text{Mn}_{0.4})\text{O}_2$  particles are completely covered with the STOBA layer. Generally, the thermal runaway of standard commercial lithium-ion batteries starts around 180 °C. However, the STOBA particles completely melt at that temperature and forms a dense conformal polymer film on the surface of the  $\text{Li}(\text{Ni}_{0.4}\text{Co}_{0.2}\text{Mn}_{0.4})\text{O}_2$  cathode.<sup>31</sup> The molten STOBA particles are expected to wet the interface and provide an ion-insulating barrier by restricting the charge transfer between the cathode and the electrolyte. Therefore, there cannot be direct electrode-electrolyte reaction and  $\text{O}_2$  will be barred from direct contact with the electrolyte, and thus prevents the cell from explosion at and above 180 °C. Unlike some commercial shutdown separators which shrink and risk the electrode shorting, the melting and formation of conformal film on the cathode surface by the STOBA material prevent any such types of battery related accidents from thermal runaway. The SEM results are also supported by the observation found in nitrogen adsorption-desorption analysis.

#### $^7\text{Li}$ MAS NMR analysis of STOBA coated cathode

$^7\text{Li}$  MAS NMR measurements were carried out to study the  $\text{Li}^+$  interaction with the STOBA coated cathode. Fig. 5 shows the  $^7\text{Li}$  MAS NMR spectra of the bare  $\text{Li}(\text{Ni}_{0.4}\text{Co}_{0.2}\text{Mn}_{0.4})\text{O}_2$  cathode and the STOBA coated  $\text{Li}(\text{Ni}_{0.4}\text{Co}_{0.2}\text{Mn}_{0.4})\text{O}_2$  cathodes without and with thermal treatment at 150 and 180 °C. All the samples were in the 100% SOC state before the measurements. The peak observed around -0.1 ppm is due to the interaction of  $\text{Li}^+$  with the oxygen atoms of the  $\text{Li}(\text{Ni}_{0.4}\text{Co}_{0.2}\text{Mn}_{0.4})\text{O}_2$  cathode. A close examination of these  $^7\text{Li}$  NMR spectra showed that there was an additional small peak observed at 136 ppm with the STOBA coated  $\text{Li}(\text{Ni}_{0.4}\text{Co}_{0.2}\text{Mn}_{0.4})\text{O}_2$  cathode. The figure in the inset shows the enlarged version of the peak at 136 ppm. The interaction of  $\text{Li}^+$  ions with the N and O of the STOBA material gives the weak peak at 136 ppm. As the amount of STOBA is only 2.0% in comparison to the amount of  $\text{Li}(\text{Ni}_{0.4}\text{Co}_{0.2}\text{Mn}_{0.4})\text{O}_2$ , the intensity of this peak is very weak. The intensity of the peak becomes weaker after the STOBA coated sample was thermally treated at 150 °C for 30 min, and it completely disappeared after thermal treatment at 180 °C. The phenomenon can be illustrated in Scheme 1. At room temperature, the STOBA layer was porous enough to allow the  $\text{Li}^+$  ions pass freely at the time of charge-discharge cycles. When the sample was thermally treated at 150 °C, the STOBA layer started to melt and blocked the pores slowly and reduced the pore volumes as confirmed from Figs. 1 and 4. Therefore, the interaction of  $\text{Li}^+$  with N and O atoms also decreases due to the presence of a less number of lithium ions in the STOBA layer, and thus presents a weaker peak at 136 ppm. Finally, when the STOBA coated  $\text{Li}(\text{Ni}_{0.4}\text{Co}_{0.2}\text{Mn}_{0.4})\text{O}_2$  sample was thermally treated at 180 °C for 30 min, the STOBA layer melted completely with no significant pores in the material, and thus blocked the charge transfer through the layer. The crosslinking and melting of the STOBA layer, triggered by thermal treatment, not only stops the  $\text{Li}^+$  ions transfer but also suppresses the moving of electrons. In such a situation,  $\text{Li}^+$  ions and electrons can possibly reside inside the  $\text{Li}(\text{Ni}_{0.4}\text{Co}_{0.2}\text{Mn}_{0.4})\text{O}_2$  cathode, as illustrated in the right part of Scheme 1.



**Scheme 1** Schematic diagram of change in morphology of STOBA layer in STOBA coated  $\text{Li}(\text{Ni}_{0.4}\text{Co}_{0.2}\text{Mn}_{0.4})\text{O}_2$  cathode after thermal treatment.

Another noticeable change in the  $^7\text{Li}$  MAS NMR spectra is the change in the linewidths of the main peak at  $-0.1$  ppm. The  $^7\text{Li}$  MAS NMR linewidth of the bare  $\text{Li}(\text{Ni}_{0.4}\text{Co}_{0.2}\text{Mn}_{0.4})\text{O}_2$  cathode at 100% SOC possesses 0.62 kHz. The linewidth increases to 2.93 kHz in the 2 wt.% STOBA coated  $\text{Li}(\text{Ni}_{0.4}\text{Co}_{0.2}\text{Mn}_{0.4})\text{O}_2$  cathode at 100% SOC. This suggests that the  $\text{Li}^+$  ions are more mobile in the bare  $\text{Li}(\text{Ni}_{0.4}\text{Co}_{0.2}\text{Mn}_{0.4})\text{O}_2$  cathode than the STOBA coated cathode. It has been reported that the discharge capacity decreases slightly with the STOBA coated cathode than the bare cathode.<sup>35</sup> These observations imply that the STOBA coating slightly influences the lithium ion mobility and may affect the overall capacity of battery. The linewidths again narrow down to 2.5 and 0.5 kHz for the STOBA coated cathode samples treated at 150 and 180 °C, respectively. As the STOBA material melts at these temperatures, the lithium ions are extruded from this layer and confined within the cathode. As a result, the lithium ions may move more freely inside this layered cathode structure which resulted narrow linewidths.

#### Solid-state $^{13}\text{C}$ CPMAS NMR analysis of STOBA

Solid-state  $^{13}\text{C}$  NMR measurements were employed to investigate the backbone structure of the STOBA material. Fig. 6 shows the  $^{13}\text{C}$  CPMAS NMR spectra of pure STOBA material and the STOBA samples thermally treated at 150 and 180 °C. The peak at 179 ppm was assigned to the carbon adjacent to the oxygen of the modified maleimide unit, while the peak at 143 ppm was assigned to the carbon from the benzene ring of STOBA (Scheme 1). The carbon of the benzene ring which attached to the nitrogen of the modified maleimide unit was observed at 131 ppm. The peak at 42 ppm was due to the methylene carbon between the two benzene rings. The peaks at 31 ppm was ascribed to the quaternary carbon attached with the methyl group of the modified maleimide unit, and the peak at 19 ppm was due to the methyl carbon attached with the modified maleimide unit. In the  $^{13}\text{C}$  CPMAS NMR spectra, a characteristic change in the peak intensity was observed for the peaks at 31 and 19 ppm. In the pure STOBA sample without thermal treatment, the peak at 31 ppm appeared as a shoulder only, while the intensity of the peak at 19 ppm was very low. When the sample was thermally treated at 150 °C for 30 min, however, the corresponding peaks became

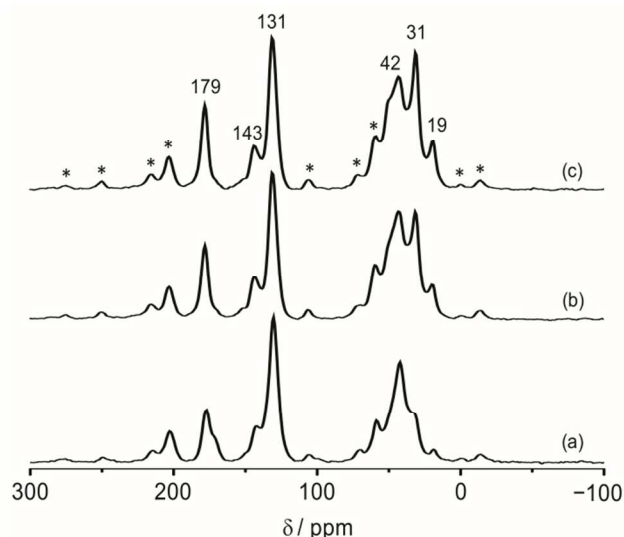


**Fig. 6**  $^{13}\text{C}$  CPMAS NMR spectra of (a) pure STOBA and the STOBA material thermally treated at (b) 150 °C and (c) 180 °C acquired at a spinning speed of 9 kHz. The spinning sidebands are marked with asterisks.

more prominent. The peak intensity was increased further and finally sharp peaks were observed for the sample thermally treated at 180 °C for 30 min. It suggested that the STOBA chains were crosslinked with each other when the temperature was increased, leading to the increase in the degree of crosslinking. As the STOBA material melted and the degree of crosslinking was increased at a higher temperature, the chains mobility was reduced and became more rigid in favor of  $^1\text{H}$  to  $^{13}\text{C}$  dipolar transfer via cross polarization to make the peaks at 31 and 19 ppm more intense. The  $^{13}\text{C}$  CPMAS NMR results are also consistent with the phenomenon described in Scheme 1.

#### Conclusions

The self-terminated oligomers with hyper branched architecture (STOBA) coated on the  $\text{Li}(\text{Ni}_{0.4}\text{Co}_{0.2}\text{Mn}_{0.4})\text{O}_2$  cathode material was studied at different temperatures to gain a deeper insight into the behavioral changes of the coating layer and to explore its possible role in suppressing thermal runaway problem in lithium ion batteries. The nitrogen adsorption-desorption analysis and SEM confirmed the change in morphology of the STOBA layer from porous to almost nonporous layer with the rise in temperature. The XPS analysis indicated mainly 2+, 3+ and 4+ oxidation states for nickel, cobalt and manganese, respectively, in the  $\text{Li}(\text{Ni}_{0.4}\text{Co}_{0.2}\text{Mn}_{0.4})\text{O}_2$  cathode material, and confirmed the deposition of STOBA material on the  $\text{Li}(\text{Ni}_{0.4}\text{Co}_{0.2}\text{Mn}_{0.4})\text{O}_2$  cathode surface as the intensities of the corresponding peaks were drastically reduced after STOBA coating. The change in resistances at high temperatures gives better understanding of the role of STOBA on preventing thermal runaway and short-circuits. The very high spinning  $^7\text{Li}$  MAS NMR spectra not only demonstrated how the local environments of the lithium ions varies at different temperatures, but also revealed the possible phase change in the STOBA-cathode interface layer that can help to suppress the thermal runaway process of Li-ion batteries. The  $^{13}\text{C}$  CPMAS NMR results confirmed the increased rigidity of the STOBA chains at a higher temperature due to melting and

enhanced crosslinking of the carbon chains. The present work gained a deeper insight into the role of the STOBA coated cathode materials, which are used to improve the safety issues of lithium-ion batteries.

## 5 Acknowledgements

The authors gratefully acknowledge the financial support from the Ministry of Science and Technology of Taiwan under the grant number NSC 102-2113-M-008-006-MY3. One of the authors, H.-M. L., acknowledges the Ph.D. scholarship (2012-C1-10 2885) from Industrial Technology Research Institute of Taiwan.

## Notes and references

<sup>a</sup> Department of Chemistry, National Central University, Chung-Li 32054, Taiwan, R.O.C. Fax: +886-3-4227664; Tel: +886-3-4275054; E-mail: hmkao@cc.ncu.edu.tw

<sup>b</sup> Material and Chemical Laboratories, Industrial Technology Research Institute, Hsinchu 31040, Taiwan, R.O.C. E-mail: JPPan@itri.org.tw

† Electronic Supplementary Information (ESI) available: [TGA curve of STOBA, XPS spectra of the STOBA coated Li(Ni<sub>0.4</sub>Co<sub>0.2</sub>Mn<sub>0.4</sub>)O<sub>2</sub> cathode with the core peaks at three different points of the sample, Histogram of the particle size of the Li(Ni<sub>0.4</sub>Co<sub>0.2</sub>Mn<sub>0.4</sub>)O<sub>2</sub> cathode, Estimation of minimum amount of STOBA to coat Li(Ni<sub>0.4</sub>Co<sub>0.2</sub>Mn<sub>0.4</sub>)O<sub>2</sub> particle]. See DOI: 10.1039/b000000x/

- 1 S. Zhang, X. Yang, Y. Numata and L. Han, *Energy Environ. Sci.*, 2013, **6**, 1443.
- 2 D. Hart, *J. Power Sources*, 2000, **86**, 23.
- 3 B. Dunn, H. Kamath and J. M. Tarascon, *Science*, 2011, **334**, 928.
- 4 M. Z. Jacobson and C. L. Archer, *PNAS*, 2012, **109**, 15679.
- 5 F. Y. Cheng, J. Liang, Z. L. Tao and J. Chen, *Adv. Mater.*, 2011, **23**, 1695.
- 6 X. L. Ji, S. Evers, R. Black and L. F. Nazar, *Nat. Commun.*, 2011, **2**, 325.
- 7 A. S. Arico, P. Bruce, B. Scrosati, J. M. Tarascon and W. Van Schalkwijk, *Nat. Mater.*, 2005, **4**, 366.
- 8 J. M. Tarascon and M. Armand, *Nature*, 2001, **414**, 359.
- 9 M. S. Whittingham, *Chem. Rev.*, 2004, **104**, 4271.
- 10 V. Etacheri, R. Marom, R. Elazari, G. Salitra and D. Aurbach, *Energy Environ. Sci.*, 2011, **4**, 3243.
- 11 J. Wen, Y. Yu and C. Chen, *Mater. Express*, 2012, **2**, 197.
- 12 P. G. Balakrishnan, R. Ramesh and T. Prem Kumar, *J. Power Sources*, 2006, **155**, 401.
- 13 Y. Yamanaka and K. Miki, US Pat. No. 6642694.
- 14 S. Nakamura, US Pat. No. 6697259.
- 15 D. Doughty and E. P. Roth, *The Electrochem Soc. Interface*, 2012, **21(2)**, 37.
- 16 T. Wei, R. Zeng, Y. Sun, Y. Huang and K. Huang, *Chem. Commun.*, 2014, **50**, 1962.
- 17 H. Wu, G. Yu, L. Pan, N. Liu, M. T. McDowell, Z. Bao and Y. Cui, *Nat. Commun.*, 2013, **4**, 1943.
- 18 G. Venugopal, *J. Power Sources*, 2001, **101**, 231.
- 19 S. -T. Myung, Y. Hitoshia and Y. -K. Sun, *J. Mater. Chem.*, 2011, **21**, 9891.
- 20 S. -H. Kim, K. -H. Choi, S. -J. Cho, E. -H. Kil and S. -Y. Lee, *J. Mater. Chem. A*, 2013, **1**, 4949.
- 21 L. Zhang, Z. Zhang, P. C. Redfern, L. A. Curtiss and K. Amine, *Energy Environ. Sci.*, 2012, **5**, 8204.
- 22 L. Zhang, Z. Zhang, H. Wu and K. Amine, *Energy Environ. Sci.*, 2011, **4**, 2858.
- 23 Q. Wang, S. M. Zakeeruddin, I. Exnar and M. Grätzel, *Electrochem. Commun.*, 2008, **10**, 651.
- 24 M. Xiong, H. Tang, Y. Wang and M. Pan, *Carbohydr. Polym.*, 2014, **101**, 1140.
- 25 S. S. Zhang, *J. Power Sources*, 2007, **164**, 351.
- 26 H. Lee, M. Yanilmaz, O. Toprakci, K. Fu and X. Zhang, *Energy Environ. Sci.*, 2014, DOI: 10.1039/C4EE01432D.

- 27 Q. Wang, J. Sun, X. Yao and C. Chen, *Electrochem. Solid-State Lett.*, 2005, **8**, A467.
- 28 H. F. Xiang, Q. Y. Jin, C. H. Chen, X. W. Ge, S. Guo and J. H. Sun, *J. Power Sources*, 2007, **174**, 335.
- 29 H. Lee, M. G. Kim and J. Cho, *Electrochem. Commun.*, 2007, **9**, 149.
- 30 L. J. Fu, H. Liu, C. Li, Y. P. Wu, E. Rahm, R. Holze and H. Q. Wu, *Solid State Sci.*, 2006, **8**, 113.
- 31 M. Baginska, B. J. Blaiszik, R. J. Merriman, N. R. Sottos, J. S. Moore and S. R. White, *Adv. Energy Mater.*, 2012, **2**, 583.
- 32 Q. Wang, P. Ping, X. Zhao, G. Chu, J. Sun and C. Chen, *J. Power Sources*, 2012, **208**, 210.
- 33 Y. Shigematsu, S. Kinoshita and M. Ue, *J. Electrochem. Soc.*, 2006, **153**, A2166.
- 34 C. -R. Yang, J. -P. Pan, C. -A. Chen and J. -M. Hsu, US Pat. No. 8137838.
- 35 C. -C. Lin, H. -C. Wu, J. -P. Pan, C. -Y. Su, T. -H. Wang, H. -S. Sheu and N. -L. Wu, *Electrochim. Acta*, 2013, **101**, 11.
- 36 <http://www.rdmag.com/RD100-Awards-Self-Terminating-Technology-Holds-Li-Ion-Energy-In-Check/>
- 37 D. P. Abraham, E. P. Roth, R. Kostecki, K. McCarthy, S. MacLaren and D. H. Doughty, *J. Power Sources*, 2006, **161**, 648.
- 38 S. Verdier, L. E. Ouatani, R. Dedryvère, F. Bonhomme, P. Biensan and D. Gonbeau, *J. Electrochem. Soc.*, 2007, **154**, A1088.
- 39 X. Bie, L. Liu, H. Ehrenberg, Y. Wei, K. Nikolowski, C. Wang, Y. Ueda, H. Chen, G. Chen and F. Du, *RSC Adv.*, 2012, **2**, 9986.